Journal of Solid State Chemistry 182 (2009) 2461–2467

Contents lists available at ScienceDirect

Journal of Solid State Chemistry

journal homepage: www.elsevier.com/locate/jssc

$PbMn(SO_4)_2$: A new chiral antiferromagnet

D.V. West [a,*], I.D. Posen [a], Q. Huang [b], H.W. Zandbergen [c], T.M. McQueen [a], R.J. Cava [a]

[a] Department of Chemistry, Princeton University, Princeton, NJ 08544, USA
[b] NIST Center for Neutron Research, Gaithersburg, MD 20899, USA
[c] Kavli Institute for Nanoscience, Technical University of Delft, The Netherlands

ARTICLE INFO

Article history:
Received 3 April 2009
Received in revised form
10 June 2009
Accepted 13 June 2009
Available online 21 June 2009

Keywords:
Acentric
Piezoelectric
Frustration
Magnetism
Chiral
New compound

ABSTRACT

$PbMn(SO_4)_2$ has been synthesized in an evacuated quartz tube. The nuclear and magnetic crystal structures have been determined using powder X-ray and neutron diffraction. This material crystallizes in the enantiomorphic space group pair $P4_12_12(\#92)$ and $P4_32_12(\#96)$, forming a double-helical arrangement of Pb^{2+} and Mn^{2+} cations. The $Mn^{2+}O_6$ octahedra are distorted. Each $3d^5$ Mn^{2+} has four nearest-neighbors and four next-nearest-neighbors adopting a frustrating arrangement. The compound orders antiferromagnetically at 5.5 K. Field dependent specific heat and magnetization measurements show that T_N is suppressed to 3.3 K when $\mu_0 H = 9$ T.

1. Introduction

Inorganic materials lacking an inversion center can exhibit dielectric phenomena such as ferro-, piezo-, and pyroelectricity [1]. These technologically important materials are used in motion detectors, to keep time in quartz watches, as capacitors in random access memory, etc. They are relatively uncommon, as the inorganic crystal structure database shows that only one out of six reported structures are acentric. Only one in four of those are chiral, making such crystal structures rare. Geometric frustration is a phenomenon whereby the satisfaction of all nearest-neighbor (NN) magnetic interactions is prevented by the spatial arrangement of the atoms. It is most typically portrayed as antiferromagnetic interactions on a triangle, where two nearest-neighbors share a third nearest-neighbor, and the three antiparallel alignments are not simultaneously possible. Competing ferro- and antiferromagnetic interactions can also give rise to magnetic frustration. This situation can lead to a degeneracy of ground states which partially or completely neutralizes the strong nearest-neighbor interactions allowing the longer-range interactions to dominate the magnetic behavior. Frustration can produce exotic magnetic ground states and has been linked to important electronic phenomena such as superconductivity [2].

This study reports the discovery of $PbMn(SO_4)_2$, a new inorganic material in the chiral and piezoelectric crystal class 422. It is the second material reported in the Pb–Mn–SO_4 phase diagram [3]. The material orders antiferromagnetically, with crystal structure considerations and physical property measurements indicating that this material may experience some degree of geometric frustration. Although no dielectric measurements were performed, such studies on this material may be of future interest from the perspective of magnetoelectric coupling.

2. Experimental

$PbMn(SO_4)_2$ was synthesized by intimately mixing stoichiometric quantities of $PbSO_4$ (reagent grade, Alfa Aesar) and $MnSO_4 \cdot H_2O$ (99%, Alfa Aesar). The mixture was placed in an open quartz tube and dried for 2 h under flowing N_2 at 420 °C. To prevent rehydration, the tube was evacuated while hot and then sealed. A single phase sample was obtained by heating the tube for two days at 850 °C, followed by three additional heatings at 750 °C for two days with intermediate grindings.

Magnetic and specific heat data were measured using a quantum design physical property measurement system (PPMS). Temperature dependent magnetization data were measured under fields ranging from $\mu_0 H = 0.1$ to 9 T in the temperature range 1.8–200 K. Specific heat data were collected from 0.3 to 30 K under fields of $\mu_0 H = 0$ and 9 T. A 30.8 mg of $PbMn(SO_4)_2$ were ground with 27.0 mg of Ag powder. The mixture was pressed into a pellet, sealed in a quartz tube and sintered for 5 min at 750 °C. An 8.5 mg piece was broken off from the pellet and used for the specific heat measurement. The Ag contribution to the specific

* Corresponding author.
E-mail address: barleytone@gmail.com (D.V. West).

0022-4596/$ - see front matter © 2009 Elsevier Inc. All rights reserved.
doi:10.1016/j.jssc.2009.06.021

heat was subtracted prior to further analysis. No portion of the C/T vs. T^2 plot ($T = 0.4$–30 K) is linear, complicating the subtraction of the lattice contribution using the low temperature Debye T^3 term. Instead, C from 25 to 30 K for $\mu_0 H = 0$ T was fit to $C = \beta_3 T^3 + \beta_5 T^5 + \beta_7 T^7$ with $\beta_3 = 5.03(6)$, $\beta_5 = -0.0054(2)$, and $\beta_7 = 2.3(1) \times 10^{-6}$ [4]. The Debye temperature, extracted from β_3, is 167 K. Support for this lattice subtraction comes from the fact that although the fit was performed in the range 25–30 K, it accurately describes the 0 T data down to 19 K. In addition, the integration of the resulting magnetic only C/T vs. T results in a calculated magnetic entropy loss close to $R\ln(6)$, the value expected for $\mathbf{S} = 5/2$, further supporting the lattice subtraction.

Nuclear and magnetic structures were characterized using X–ray and neutron diffraction performed on polycrystalline samples. Powder X-ray diffraction (PXRD) data were collected at room temperature with a Bruker D8 Focus, using Cu$K\alpha$ radiation

Table 1
Structural data for $PbMn(SO_4)_2$ from NPD at 298 and 15 K, space group $P4_32_12$.

$PbMn(SO_4)_2$		298 K				15 K			
Atom	Site symmetry	x	y	z	B_{iso}	x	y	z	B_{iso}
Mn	4*a*	0.8326(4)	0.8326(4)	0	0.94(7)	0.8344(3)	0.8344(3)	0	0.17(4)
Pb	4*a*	0.2516(2)	0.2516(2)	0	1.32(3)	0.2519(2)	0.2519(2)	0	0.38(2)
S1	8*b*	0.1734(5)	0.2467(6)	0.7427(3)	0.72(6)	0.1737(4)	0.2454(4)	0.7437(2)	0.12(4)
O1	8*b*	0.3406(3)	0.3878(3)	0.7372(2)	1.18(4)	0.3397(2)	0.3892(2)	0.7357(1)	0.46(2)
O2	8*b*	0.1699(4)	0.1234(4)	0.6554(1)	1.38(5)	0.1689(3)	0.1210(3)	0.6557(1)	0.51(3)
O3	8*b*	0.9909(3)	0.3604(4)	0.7549(2)	1.91(5)	0.9902(2)	0.3601(3)	0.7557(1)	0.62(3)
O4	8*b*	0.2072(3)	0.1164(4)	0.8269(2)	1.35(5)	0.2100(2)	0.1154(3)	0.8277(1)	0.62(3)
Lattice parameters									
		a	6.7497(1) Å			a	6.7331(1) Å		
		c	13.7639(3) Å			c	13.7435(2) Å		
Fit statistics									
		χ^2	1.46			χ^2	1.60		
		$R(F^2)$	5.15%			$R(F^2)$	2.76%		
		R_p	4.64%			R_p	4.41%		
		R_{wp}	5.67%			R_{wp}	5.48%		

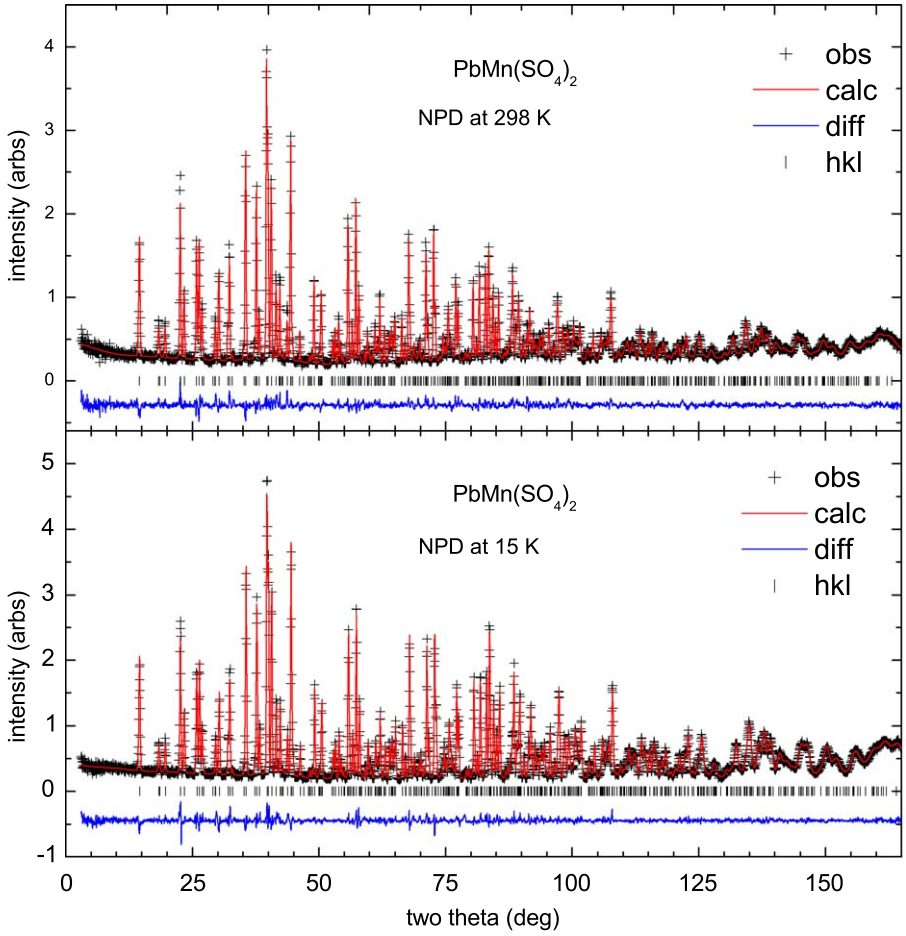

Fig. 1. Refinement of $PbMn(SO_4)_2$ against NPD at 298 (top) and 15 K (bottom).

and a graphite diffracted beam monochromator. The unit cell of $PbMn(SO_4)_2$ was auto-indexed using the TREOR algorithm [5]. Neutron powder diffraction (NPD) data were collected at the NIST Center for neutron research on the high resolution powder neutron diffractometer (BT–1) with neutrons of wavelength 1.5403 Å produced by using a Cu(311) monochromator. Collimators with horizontal divergences of 15, 20 and 7 min of arc were used before and after the monochromator and after the sample, respectively. Data were collected at 1.6, 6, 15 and 298 K in the 2θ range of 3°–168° with a step size of 0.05°. The structural parameters were determined by Rietveld refinement of the neutron diffraction data using the GSAS program [6,7]. The atomic neutron scattering factors used in the refinements for Pb, Mn, S, and O were 0.940, −0.375, 0.285 and 0.581×10^{-12} cm, respectively. The magnetic form factor coefficients used for Mn^{2+} were taken from the International Tables for Crystallography [8]. Magnetic moment magnitudes were restrained to the expected value of 5 μ_B with a standard deviation of 0.01 μ_B.

3. Results and discussion

3.1. Crystal structure

PXRD indicates a single phase sample for $PbMn(SO_4)_2$. The pattern was indexed to a tetragonal unit cell with lattice parameters of $a = 6.753$ Å and $c = 13.770$ Å. A unit cell stoichiometry of $Pb_4Mn_4(SO_4)_8$ was assigned from the ratio of the unit cell

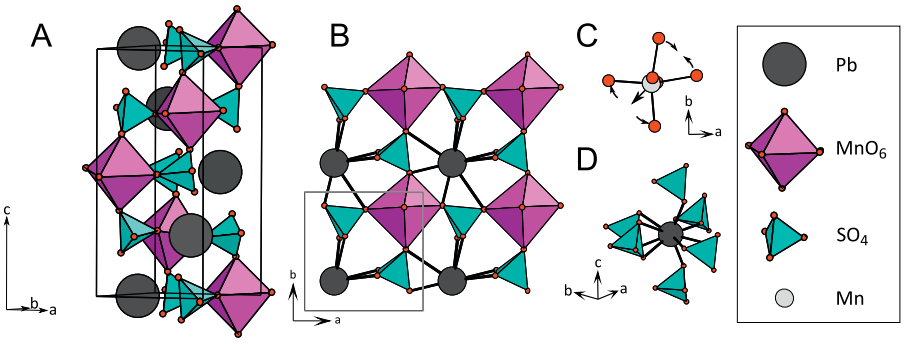

Fig. 2. (A) The crystal structure of $PbMn(SO_4)_2$ has 4 MnO_6 octahedra, 8 SO_4 tetrahedra per unit cell and a double helical arrangement in which Pb^{2+} and Mn^{2+} cations wind around each other, (B) a single tetragonal layer is shown. There are 4 such identical layers per unit cell related by a 4-fold screw axis, (C) the MnO_6 octahedra share a single oxygen with 6 SO_4 tetrahedra. The Mn is displaced off the ideal octahedral center towards an edge, and (D) the Pb's are coordinated by 10 oxygens, 2 from each of the 4 SO_4 within the same tetragonal layers, and 1 each from an SO_4 in the layers above and below.

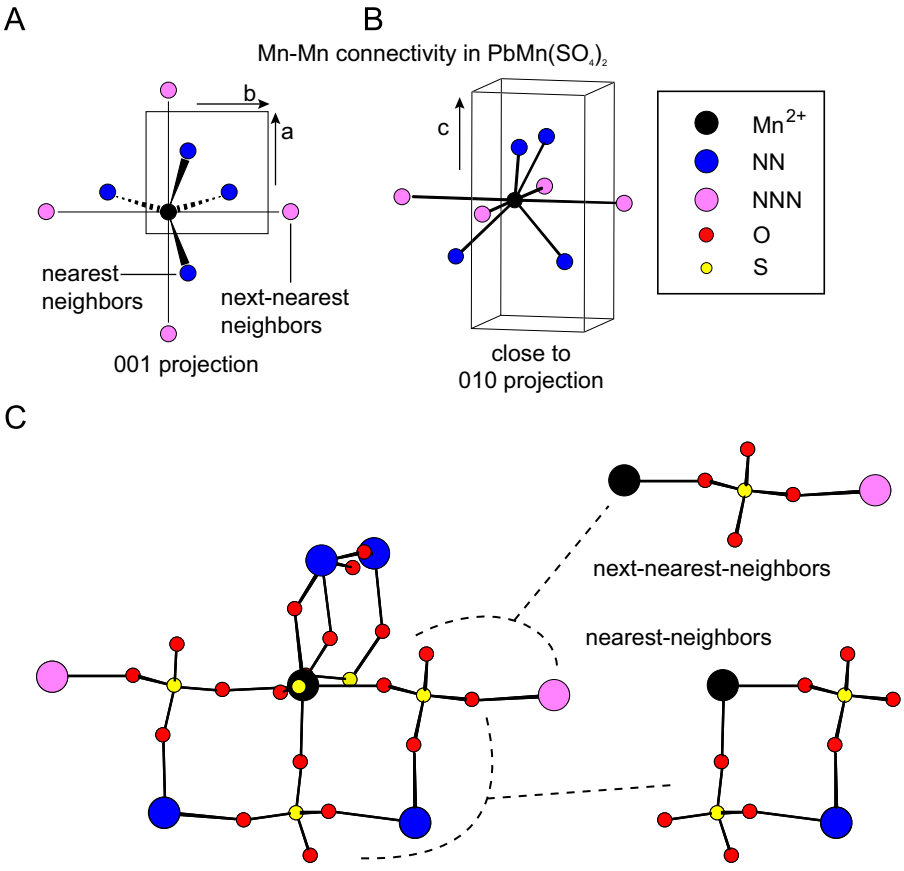

Fig. 3. (A, B) Each Mn has 4 NN's, 2 in the layer above, and 2 in the layer below. Mn's also have 4 NNN's, all within the same tetragonal layer. A pair of NN's are NNN's to eachother and (C) NN's are connected by 2 Mn–O–S–O–Mn right angle pathways while NNN's are connected by a single Mn–O–S–O–Mn straight pathway.

volume (627.9 Å^3) to the sum of the molar volumes of $PbSO_4$ (80.335 Å^3) and $MnSO_4 \cdot$ (72.435 Å^3), equal to 4.11.

Crystal-chemical reasoning was used to solve the crystal structure from PXRD. The unit cell dimensions, the tetragonal symmetry and the stoichiometry strongly suggest a structure with four layers each possessing two metal cations. Centrosymmetric arrangements of the Pb^{2+} and Mn^{2+} did not provide a good match to the diffraction data. Chiral space groups were therefore tested. There are two tetragonal enantiomorphic space group pairs with 4-fold screw axes: space group numbers 91 and 95 ($P4_122$ and $P4_322$), and also 92 and 96 ($P4_12_12$ and $P4_32_12$). While models in both pairs produce similar crystal structures, it was found that the additional reflection condition of $0\,k\,0$, $k = 2n$, found only in the second pair, was necessary for a perfect match to the data as models consistent with the first pair predicted diffraction intensity where no peaks were observed in the data. The final refinements were done in $P4_32_12$ with the understanding that the powder is likely a mix of both enantiomorphs. Precise structural parameters were determined by refinement against NPD data at 298 and 15 K (Table 1, Fig. 1).

Free refinement of all atomic positions yields a rational structure with SO_4 tetrahedra, MnO_6 octahedra and a double-helical winding of the metal cations around each other (Fig. 2A). The unit cell is made of four layers that are crystallographically identical, related to one another by the four-fold screw axis. One of these tetragonal layers is shown in Fig. 2B. The Mn position is displaced from the ideal octahedral center towards an edge (Fig. 2C). Each Pb^{2+} has 10-fold coordination, sharing two oxygens with four SO_4 groups within the tetragonal layers, and sharing a single oxygen with one SO_4 in the plane above, and one in the plane below (Fig. 2D).

The Mn–Mn connectivity, important for understanding the magnetic structure and properties, is shown in Fig. 3. Each Mn is crystallographically identical, and has four nearest-neighbor and four next-nearest neighbor (NNN) Mn atoms. Any given Mn and its four NNN's all lie within the same tetragonal layer, forming a 2D square net. The NN's, however, are divided in pairs, with two NN's in the tetragonal plane above, and two in the plane below, forming a distorted tetrahedron around the central Mn (Fig. 3A and B). The Mn atoms within these pairs are NNN's to each other. A Mn is connected to its NN's by two Mn–O–S–O–Mn pathways that have a ~90° type arrangement (Fig. 3C). The NNN connectivity has a single Mn–O–S–O–Mn pathway that is a 180° type layout. This arrangement may be frustrating depending upon the signs and strengths of the NN and NNN superexchange interactions.

3.2. Magnetic structure and properties

The magnetic susceptibility at $\mu_0 H = 0.1$ T (Fig. 4) exhibits Curie–Weiss behavior above 6 K with $\theta_{CW} = -10.7$ K and $p_{eff} = 6.2\,\mu_B$, close to the expected 5.9 μ_B for $\mathbf{S} = 5/2$ systems [9]. An antiferromagnetic transition is observed with $T_N = 5.5$ K. The magnetic transition (Fig. 5) was suppressed by a field, reaching 3.5 K when $\mu_0 H = 9$ T. M vs. H curves are shown in Fig. 6. The first derivatives of these curves at fields below 1 T display a kink that systematically shrinks with increasing temperatures, and is gone by the T_N at 5.5 K (Fig. 6 inset). This feature is indicative of a subtle field-induced effect, and may reflect a weak ferromagnetic component in the magnetically ordered phase. There is an additional S-like feature in the M vs. H data at fields between 5 and 8 T, seen most clearly in the 3.5 and 4.5 K data. This indicates the presence of another field-induced transition, possibly of the spin-flop type. Specific heat measurements under fields of 0 and 9 T show anomalies which peak at 5.4 and 3.3 K respectively, corresponding well to the magnetization data. The anomaly is not

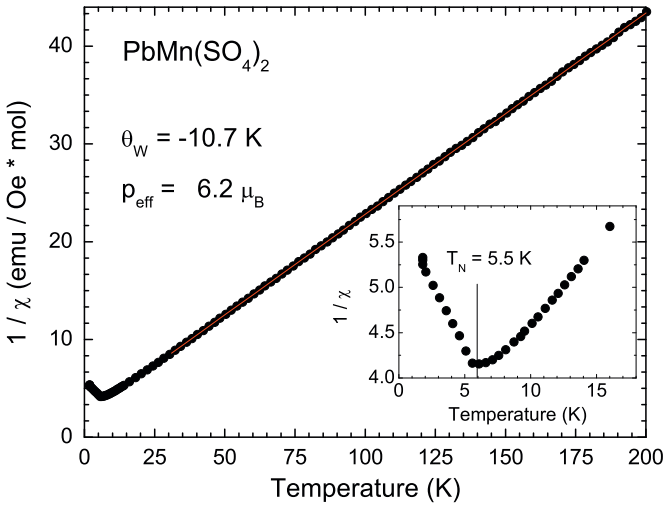

Fig. 4. The $1/\chi$ vs. T curve showing Curie-Weiss behavior and an antiferromagnetic transition at 5.5 K.

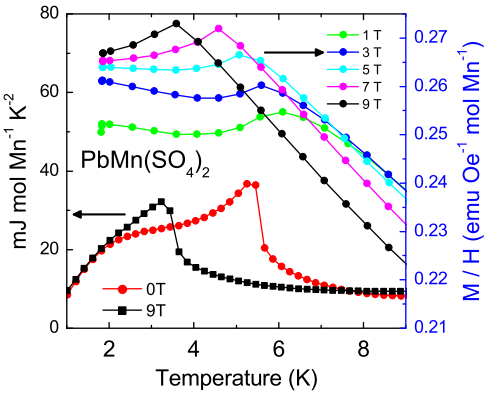

Fig. 5. Several χ vs. T curves under fields ranging from $\mu_0 H = 1$–9 T, and C/T vs. T curves under fields of $\mu_0 H = 0$ and 9 T.

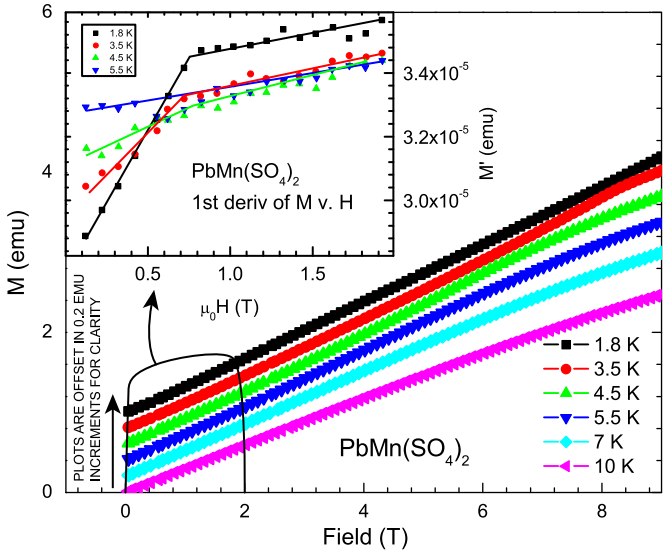

Fig. 6. M vs. H curves at increasing temperatures. The curves are offset along the y-axis in increments of 0.2 emu for clarity. (inset) There is a kink in the first derivative at low fields that decreases systematically with increasing temperatures, indicative of subtle field-induced effect, and there is an S-like feature at higher fields in M vs. H, seen most clearly in the 3.5 and 4.5 K data. Lines are drawn to guide the eye.

lambda-like, as is seen for example in Mn^{2+} salts such as $MnCl_2 \cdot 4H_2O$ [10], but rather has a sharp feature at higher temperatures followed by a second feature at lower temperatures, near 5.4 and 2.5 K, respectively, in the zero field data. This may reflect the fact that the geometric frustration results in the ordering of NN and NNN spins at different temperatures. The phonon contribution was modeled and then subtracted (see experimental section) to yield an approximation to the magnetic only specific heat, and thus, entropy loss upon ordering. Up to 30 K under 0 and 9 T fields, the magnetic entropy change limits to a value close to $R\ln(6)$, the value expected for $\mathbf{S} = 5/2$ systems (Fig. 7). This indicates that all spins in the system are in their lowest energy states by the lowest temperature of the specific heat measurement, 1.6 K. The overall magnetic and specific heat data reflect a subtle balance among different kinds of magnetic interactions in $PbMn(SO_4)_2$, and suggest that this material if studied in detail in future work would display a complex temperature-field-orientation magnetic phase diagram, typical of systems where geometric magnetic frustration plays a significant role in the properties.

Low temperature NPD was employed to further investigate the magnetic ordering. At 1.6 K, the sample exhibits long-range magnetic order indexable by a $2a \times 2b \times c$ supercell of the nuclear structure, suggesting antiferromagnetic alignment within the tetragonal planes. The basic magnetic structure was solved by a combined nuclear and magnetic model refinement against the 1.6 K diffraction pattern using $P1$ as the magnetic space group. The nuclear positions and thermal parameters were fixed at the 15 K values, minimizing the number of freely refineable parameters. It was found that no refinement even qualitatively matched the data unless all NNN alignments were close to antiparallel, thus forming square antiferromagnetic nets (Fig. 8). This is logical, given the doubled a and b axes of the magnetic unit cell. This NNN

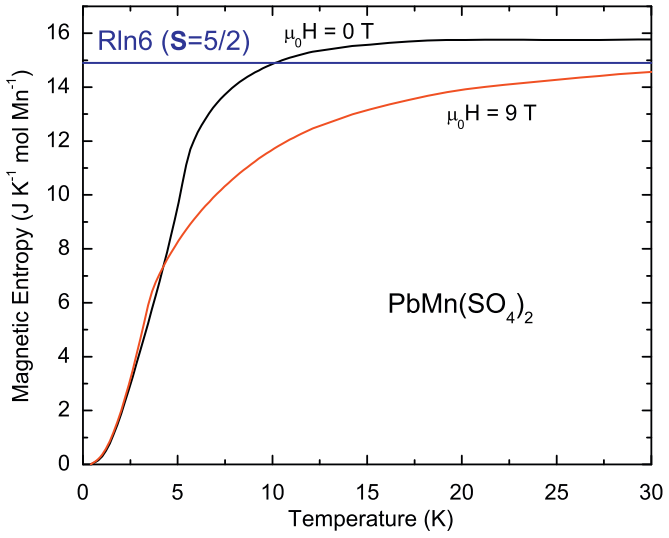

Fig. 7. Magnetic entropy loss under fields of $\mu_0 H = 0$ and 9 T. Both curves limit to a value close to $R\ln(6)$, the expected value for $\mathbf{S} = 5/2$ systems.

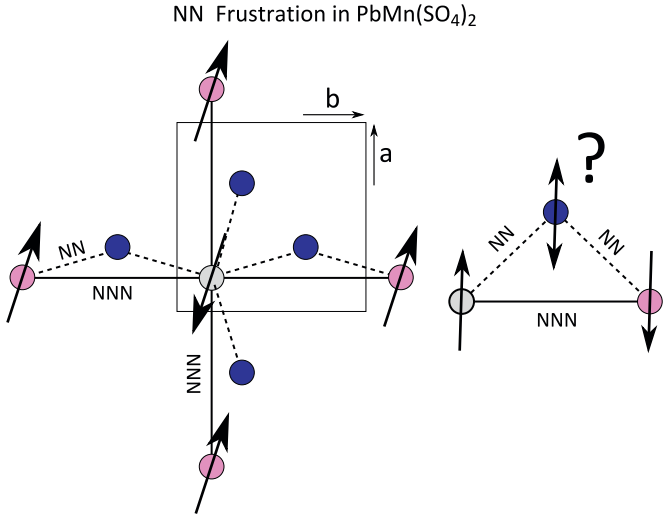

Fig. 8. The magnetic unit cell has doubled a and b axes, strongly suggesting square antiferromagnetic nets within the tetragonal planes. Antiparallel alignment of the NNN's yields a degeneracy with respect to NN alignments, otherwise known as geometric frustration.

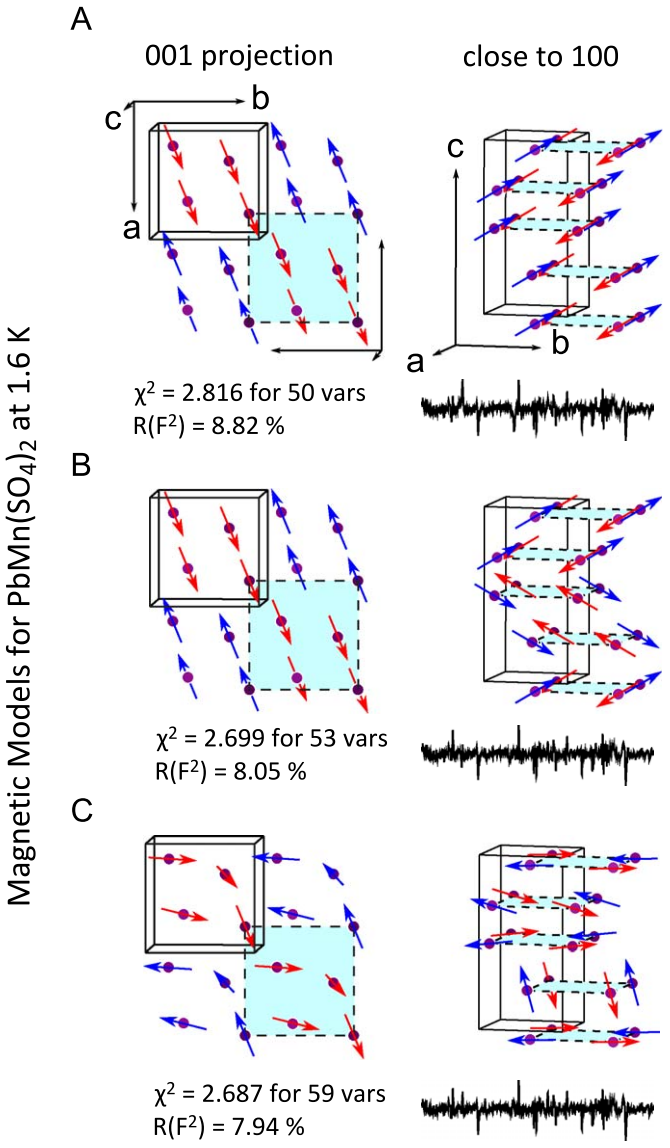

Fig. 9. The magnetic structure contains antiferromagnetic square nets within the tetragonal planes. The exact relationship between adjacent planes is unclear from the current refinements: (A) a magnetic model for which every moment is constrained to be parallel or antiparallel to a given vector, (B) a model in which all X and Y components are constrained to be parallel or antiparallel to a given vector, but the Z components are allowed to vary. The tetragonal planes are still constrained to be antiferromagnetic square nets, and (C) a model with no constraints other than tetragonal planes must be antiferromagnetic square nets. Below each of the models are shown the fit statistics and difference plots.

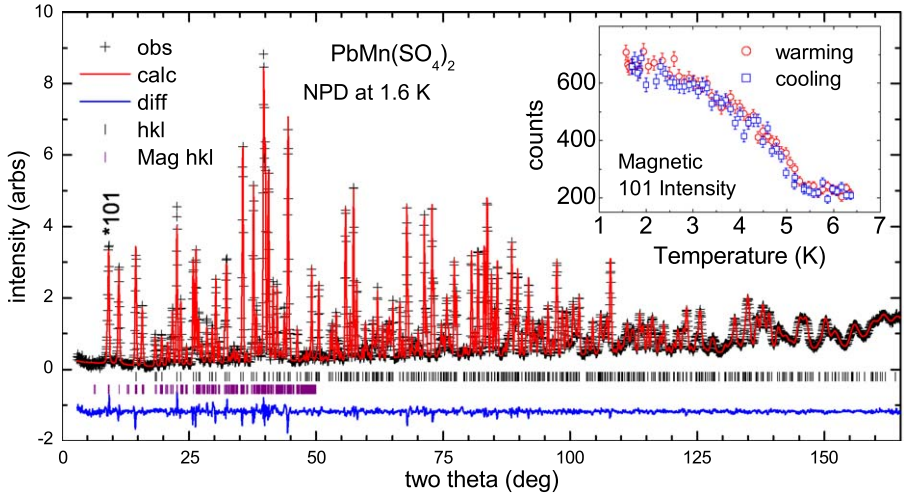

Fig. 10. A 1.6 K refinement of $PbMn(SO_4)_2$ using the nuclear model at 15 K and the magnetic model shown in Fig. 8b.

alignment gives rise to a degeneracy with respect to the NN alignments. As described above, every Mn has a pair of NN's in the plane above, and a pair of NN's in the plane below. The Mn atoms within each pair are NNN's to each other. Therefore, due to the established NNN antiferromagnetic coupling, the two NN's in a given pair will be aligned antiparallel with respect to each other, and a two-fold degeneracy exists regarding which of the NN's of a Mn is aligned "up" and which is "down" (Fig. 8). This type of degeneracy is the hallmark of geometric magnetic frustration. Calculations to investigate the signs and relative strengths of the NN and NNN magnetic interactions may be of interest to determine what role if any magnetic frustration may play in this new crystal structure type.

Despite the degeneracy in the NN alignment, the specific heat data indicate that the magnetic ordering is complete by 1.6 K. Three different magnetic models are shown in Fig. 9, each with varying levels of constraints between moments in adjacent planes. The model in Fig. 9A has all moments constrained to be either parallel or antiparallel to a common vector. The model in Fig. 9B maintains perfect NNN antiparallel alignment. In addition, the x and y components of every moment are constrained to be parallel or antiparallel to a common vector while the z components are freely refined for each layer. The model in Fig. 9C only constrains all NNN's to be antiparallel with no defined relationship between the layers. A model without constraints has 16 independent magnetic moments, but the refinement of such a model is not stable. However, with maximum damping of the magnetic moment vectors and additional Marquardt damping, this refinement produces a structure that is very similar to the model shown in Fig. 9C. All refined models showed similar fit statistics, and visual inspection of the difference plots shows their fits to be quite similar. As such, the nature of the ordering along the c axis is not clear from these data. A combined magnetic and nuclear structure refinement using the model from Fig. 9B is shown in Fig. 10. Measurement of the magnetic scattering as a function of temperature confirms that long-range order onsets at 5.5 K, consistent with the magnetization and specific heat data (Fig. 10, inset). Magnetic fit statistics at 1.6 K, based on magnetic-only scattering approximated by subtracting the 15 K data from the 1.6 K data, and using the magnetic models determined from the combined refinements were $\chi^2 = 16$, $R_p = 9.6\%$, $R_{wp} = 16\%$, $R(F^2) = 24\%$. Finally, we note that because the underlying nuclear positions are chiral, there should be two enantiomorphic magnetic structures present, both with $P1$ symmetry. However, it is not possible to tell them apart with powder diffraction data, and may even be difficult with single crystal data.

If the NNN alignments are perfectly antiparallel, and only NN and NNN interactions are significant, then there is no energetic difference in the Heisenberg model between any of the possible NN alignments. Strict NNN antiferromagnetic alignment perfectly frustrates the NN alignment, regardless of the sign of the interaction. Given such considerations, the models shown in Fig. 9 cannot be completely right, and particularly not the model in Fig. 9a for which half of the NN alignments are ferromagnetic, and the other half are antiferromagnetic. No thermodynamic explanation exists for such an ordering. As such, it is possible that the NNN alignments are only imperfectly antiparallel, thereby allowing the non-degenerate ground state that is indicated by the specific heat data. Another possibility is that longer range interactions, such as the next-next-nearest-neighbors, are significant enough to give a non-degenerate ground state below 5.5 K. Single crystal experiments and field dependent powder neutron scattering may help to further elucidate the ordered magnetic structure.

4. Conclusion

The new material $PbMn(SO_4)_2$ has been synthesized and its crystal structure solved using powder diffraction techniques. It adopts a rare chiral structure in the pair of enantiomorphic space groups $P4_12_12$ and $P4_32_12$ in which the Pb^{2+} and Mn^{2+} cations form a double helix along the c axis. Magnetization data indicate antiferromagnetic ordering at 5.5 K with non-trivial behavior at low temperatures in an applied field. The low temperature magnetic structure, a $2a \times 2b \times c$ supercell of the nuclear structure, has been shown to be made of NNN's aligned antiferromagnetically forming square antiferromagnetic nets within the tetragonal planes. The NN alignments have a degeneracy arising from geometric frustration. The exact nature of the spin alignment between adjacent tetragonal planes is unclear, requiring further study, and a full magnetic phase diagram would likely be of significant interest.

Acknowledgments

This research was supported by the NSF program in Solid State Chemistry, Grant no. NSF DMR-0703095. Certain commercial materials and equipment are identified in this report to describe the subject adequately. Such identification does not imply recommendation or endorsement by the NIST, nor does it imply

that the materials and equipment identified are necessarily the best available for the purpose. T. M. McQueen gratefully acknowledges support of the National Science Foundation Graduate Research Fellowship Program.

Appendix A. Supplementary Material

Supplementary data associated with this article can be found in the online version at doi:10.1016/j.jssc.2009.06.021.

References

[1] P. Halasyamani, K. Poeppelmeier, Chem. Mater. 10 (1998) 2753–2769.
[2] N.P. Ong, R.J. Cava, Science 305 (2004) 52–53.
[3] D.V. West, T.M. McQueen, I.D. Posen, X. Ke, Q. Huang, H.W. Zandbergen, A.J. Williams, P. Schiffer, R.J. Cava, J. Solid State Chem. 182 (2009) 1343–1350.
[4] A. Tari, The Specific Heat of Matter at Low Temperatures, first ed., Imperial College Press, 2003.
[5] P. Werner, L. Eriksson, M. Westdahl, J. Appl. Crystallogr. 18 (1985) 367–370.
[6] A.C. Larson, R.B. Von Dreele, Los Alamos National Laboratory Report LAUR (2000) 86–748.
[7] B.H. Toby, J. Appl. Crystallogr. 34 (2001) 210–213.
[8] E. Prince, International Tables for Crystallography, Volume C: Mathematical, Physical and Chemical Tables, third ed., Springer, Berlin, 2004.
[9] N.W. Ashcroft, N.D. Mermin, Solid State Physics, Thomson Learning, USA, 1976.
[10] W.F. Giauque, R.A. Fisher, G.E. Brodale, E.W. Hornung, J. Chem. Phys. 52 (1970) 2901–2918.